MRI signature in a novel mouse model of genetically induced adult oligodendrocyte cell death

Mueggler, T ; Pohl, H ; Baltes, C ; Riethmacher, D ; Suter, U ; Rudin, M

DOI: https://doi.org/10.1016/j.neuroimage.2011.09.001

MRI signature in a novel mouse model of genetically inducedadult oligodendrocyte cell death

Thomas Mueggler[a,1], Hartmut Pohl[b], Christof Baltes[a], Dieter Riethmacher[c], Ueli Suter[b], Markus Rudin[a,d,]

[a]Institute for Biomedical Engineering, University and ETH Zurich, Zurich, Switzerland
[b]Institute for Cell Biology, Department of Biology, ETH Zurich, Zurich, Switzerland
[c]Human Genetics Division, Southampton University School of Medicine, Southampton, United Kingdom
[d]Institute of Pharmacology and Toxicology, University Zurich, Zurich, Switzerland

Correspondence: Markus Rudin, PhD, Prof.
Institute for Biomedical Engineering, University and ETH Zurich
Institute of Pharmacology and Toxicology, University of Zurich
HIT E.22.4
Wolfgang Pauli Strasse 27
CH-8093 Zurich, Switzerland
Phone: +41 44 633 7604
Fax: +41 44 633 1187
Email: rudin@biomed.ee.ethz.ch

[1]Present address: F. Hoffmann-La Roche Ltd.
Pharma Research and Early Development
Preclinical Translational Neuroscience
CH-4070 Basel, Switzerland.
Phone: +41 61 687 4027
Email: thomas.mueggler@roche.com

Abstract

Two general pathological processes contribute to multiple sclerosis (MS): acute inflammation and degeneration. While magnetic resonance imaging (MRI) is highly sensitive in detecting abnormalities related to acute inflammation both clinically and in animal models of experimental autoimmune encephalomyelitis (EAE), the correlation of these readouts with acute and future disabilities has been found rather weak. This illustrates the need for imaging techniques addressing neurodegenerative processes associated with MS.

In the present work we evaluated the sensitivity of different MRI techniques (T2 mapping, macrophage tracking based on labeling cells in vivo by ultrasmall particles of iron oxide (USPIO), diffusion tensor imaging (DTI) and magnetization transfer imaging (MTI)) to detect histopathological changes in a novel animal model making use of intrinsic, temporally and spatially controlled triggering of oligodendrocyte cell death. This mouse model allows studying the MRI signature associated to neurodegenerative processes of MS in the absence of adaptive inflammatory components that appear to be foremost in the EAE models. Our results revealed pronounced T2 hyperintensities in brain stem and cerebellar structures, which we attribute to structural alteration of white matter by pronounced vacuolation. Brain areas were found devoid of significant macrophage infiltration in line with the absence of a peripheral inflammatory response. The significant decrease in diffusion anisotropy derived from DTI measures in these structures is mainly caused by a pronounced decrease in diffusivity parallel to the fiber indicative of axonal damage. Triggering of oligodendrocyte ablation did not translate into a significant increase in radial diffusivity. Only minor decreases in MT ratio have been observed, which is attributed to inefficient removal of myelin debris.

Key words

Axonal injury, oligodendrocyte cell death, demyelination, magnetic resonance imaging, mouse brain, T_2 hyperintensities, diffusion tensor imaging

Abbreviations

BBB, blood–brain barrier; CNS, central nervous system; DTI, diffusion tensor imaging; EAE, experimental autoimmune encephalomyelitis; FA, fractional anisotropy; MRI, Magnetic Resonance Imaging; MS, multiple sclerosis; MTR, magnetization transfer ratio; MTI, magnetization transfer imaging; PLP, Proteolipid Protein; ROI, region of interest; T_1, longitudinal relaxation time; T_2, transverse relaxation time; TAM, tamoxifen; USPIO, ultra-small particles of iron oxide; $\lambda_{\parallel}$, axonal diffusivity coefficient; $\lambda_{\perp}$, radial diffusivity coefficient.

1. Introduction

MS is commonly thought to involve two general pathological processes: acute inflammatory demyelination and axonal degeneration, though the relationship between these aspects is not fully investigated. The complex inflammatory cascade of lesion development includes T-cell and macrophage recruitment, BBB breakdown, demyelination, axonal damage, remyelination and gliosis (Prineas, 1984; Lassmann, 2005; Ludwin, 2006; Frohman et al., 2006). It has become clear that measures of acute inflammation are poor predictors of long-term disability.

Magnetic resonance imaging (MRI) is considered one of the most sensitive techniques for diagnosis of the disease (Filippi et al., 2009; Bakshi et al., 2008; Leist and Marks, 2010). Due to their sensitivity to detect early pathological events and hence their potential prognostic value, MRI readouts such as gadolinium-enhanced MRI assessing blood-brain barrier leakage and transverse relaxation time (T2)-weighted MRI assessing edema formation in conjunction with inflammatory processes have become essential components of the MS diagnosis process (Leist and Marks, 2010 *and refs therein*). Nevertheless, MRI suffers from several limitations with regard to MS diagnosis. In MS, lesions occurring include acute lesions as a result of an immune response mediated by monocytes and leukocytes, lesions characterized by oligodendrogliopathy or apoptosis, and remyelinated shadow plaques (Lassmann et al., 2001; Barnett and Prineas, 2004, Patrikios et al., 2006). Due to this heterogeneity and the complex interplay between inflammatory and degenerative processes, the histopathological correlates of MRI signal alterations are still poorly defined. This is reflected in the so-called 'clinico-radiological paradox' in MS (Barkhof et al., 2002), which refers to discrepancies between the disease burden as visualized by MRI and the extent of disability of patients. In order to improve the correlation between radiological disease markers and clinical status, a stronger weighting of neurodegenerative rather than primary inflammatory readouts has been suggested.

MRI magnetization transfer ratio (MTR), which measures the exchange between bulk water and water bound to macromolecules, is considered a measure of the macromolecular structure (Wolff et al., 1989) and myelin water fraction (Whittall et al., 1997), both potential measures of the degree of the myelination and the integrity of the myelin sheath. Diffusion tensor imaging (DTI) assessing directional diffusivity (Basser et al., 1994) might serve as an indicator of axonal integrity. Both MTR and DTI are linked to the neurodegenerative component of the disease (*for review see* Bakshi et al., 2008; Filippi et al., 2009) and complement the established MRI readouts of inflammation.

Animal models play a central role in the validation of clinical readouts as they allow direct correlation of radiological and histopathological findings. Not surprisingly, the various MRI methods have been applied to characterize animal models of MS such as rat and mouse models of experimental autoimmune encephalomyelitis (EAE). These models display disseminated and variable focal lesions at brain or spinal cord level (*for review see* Lassmann, 2008), which are difficult to interpret when using conventional T1– and T2-weighted MRI techniques sensitive for inflammatory processes only (Nessler et al., 2007; Serres et al., 2009). Therefore, in parallel to the clinical situation both DTI and

MTR measures are currently being investigated as measures of demyelination, axonal damage or myelin integrity in EAE (Budde et al., 2008; Budde et al., 2009; DeBoy et al., 2007; Serres et al., 2009; Rausch et al., 2003; Rausch et al., 2009) and CNS demyelination and remyelination in a mouse model of cuprizone-mediated demyelination (Sun et al., 2006; Zaaraoui et al., 2008). Furthermore, the use of ultra-small particles of iron oxide (USPIOs) to visualize macrophage infiltration has been proposed as refined marker for inflammatory events in MS and animal models thereof (Dousset et al., 1999a; Rausch et al., 2003; Floris et al., 2004; Berger et al., 2006; Brochet et al., 2006; Ladewig et al., 2009).

Here we describe the MRI characterization of a novel mouse model of oligodendrogliopathy (Pohl et al., 2011) that has been generated using transgene mediated, intrinsic, temporally and spatially controlled triggering of oligodendrocyte cell death. This ablation of oligodendrocytes was achieved by selective inducible expression of diphtheria toxin fragment A (DT-A) in proteolipid protein (PLP)-positive myelinating glia. The resulting pathology is characterized by a well-defined time course of myelin damage, which in turn resulted in a widespread status spongiosus of the myelin and axonal damage without involvement of adaptive immune cells. As the mouse model essentially lacks an inflammatory component, it should help identifying histopathological correlates accounting for MRI signal alteration associated to demyelination. Our objective was therefore to evaluate the sensitivity of various MRI readouts in

characterizing the pathology. Assessment of clinical signs with a defined scoring procedure over the time course of disease development showed first incidence around 2 weeks after a 5-day consecutive treatment with tamoxifen to induce DT-A expression. We quantitatively assessed T2-values, changes in T2 as a consequence of CNS infiltration of USPIO carrying macrophages as indicator of an adaptive immune response, anisotropic water diffusion properties as marker of axonal integrity, and MTR as marker of myelin content in diseased mice prior to the occurrence of clinical impairments and at end stage of pathology.

2. Methods

2.1 Animals

The transgenic mouse model was generated by crossing a mouse line expressing a tamoxifen inducible cyclic recombinase (Cre) under the PLP promoter active in oligodendrocytes (Leone et. al., 2003) with mice expressing DT-A after Cre-mediated recombination (Brockschnieder et al., 2004) allowing spatially and temporally controlled cell ablation (Pohl et al., 2011). Induction of DT-A expression was achieved by intraperitoneal (i.p.) injection of 2 mg TAM dissolved in a sunflower oil / ethanol mixture (10:1), for 5 consecutive days (start at day 1). For validation of MRI readouts male and female animals

of 19-22 g body weight have been used. Animals were housed under a normal light/dark cycle (12:12 h) with standard rodent chow and tap water ad libitum.

2.2 Scoring

Mice were monitored regularly and their impairment scored with a specially developed clinical scoring based on appearance of clinical signs modeled to reflect scorings used in EAE (Matthaei et al., 1989) in severity of occurrence: Score 0 = no observable clinical signs; score 1 = tremor and ataxia, broadened gait and reduced grip strength; score 2 = severe hind limb weakness plus pronounced ataxia and tremor; score 3 = animals temporarily fail to maintain upright position and both front and hind limbs showed severe weakness. Transition states were scored with half steps.

2.3 Animal preparation for MRI acquisition

Mice were anesthetized using 1.8 % isoflurane in an oxygen/air (20/80 %) mixture applied via a face-mask with integrated tooth-bar and placed on water-heated cradle. Body temperature was monitored using a rectal probe coupled to a fluoroptic module (QUASYS AG, Cham, Switzerland) and kept constant at 37±0.5°C. Ear bars secured reproducible positioning and reduced motion artifacts. After completion of MRI studies all animals were sacrificed by transcardial perfusion fixation and brain was removed for histological analysis. All experiments were carried out in strict adherence to the Swiss Law for Animal Protection, approved by the veterinary office of the canton of Zurich, Switzerland.

2.4 MRI

MRI experiments were carried out with a Pharmascan 47/16 system (Bruker BioSpin MRI, Ettlingen, Germany) using a birdcage transmit-receive coil for quantitative T2 and MTR measurements and a cryogenic transmit-receive radiofrequency (RF) surface coil (Ratering et al., 2008) for DTI studies. Quantitative T2 values were obtained using a multi spin echo (SE) sequence with the parameters: field-of-view (FOV) = 19x19 mm2; matrix dimension (MD) = 132x132; spatial resolution = 144x144 μm2; repetition time (TR) = 2000 ms; echo spacing (TE) = 10 ms; number of echoes: 14; number of averages (NA) = 6 and slice thickness (SLTH) = 0.8 mm. Diffusion-tensor Imaging: For DTI a multi-slice spin echo-echo planar imaging (EPI) sequence was used with: number of slices (NSL) = 15; SLTH = 0.5 mm; interslice gap = 0.25 mm; FOV = 20x15 mm2; MD = 133x100; TE = 28.3 ms, TR = 3000 ms; b-values = 1000 s/mm2 with 30 diffusion encoding directions. High resolution anatomical images were acquired using a standard spin echo rapid acquisition with relaxation enhancement (SE-RARE) sequence (Hennig et al., 1986) with FOV = 20x18.4 mm2; MD = 256x256; in plane resolution of 78x72 μm2; TE = 12 ms; TR = 3500 ms; effective echo time (TEeff) = 36 ms; RARE factor = 8; NA = 7; SLTH = 0.800 mm; NSL = 9. MTI was performed using a 3D-gradient echo (GE) sequence with FOV = 15x15x12 mm3; MD: 60x60x48; isotropic voxel dimension of 250 μm3; TE = 2 ms; TR = 30.0 ms; flip angle: 30°. A Gaussian pulse with pulse length of 1 ms, a B1 amplitude of 80 μT and an

offset frequency of 5 kHz was used for saturation of the bound water fraction. The reference sequence was obtained using the same parameters without application of the saturation pulse.

2.5 Study design:

T2 maps have been recorded from twelve mice, eight of which received i.p. injection of TAM (i.p. 2 mg; +TAM) while four littermates were used as control (no TAM injection: -TAM). In order to investigate potential alterations in macromolecular structure this group was further split, with half of the animals subjected to MTR. T2 and MTR maps were recorded at day 2 and 9 (baseline) as well as on day 37 and 41 (end stage) following TAM injection. The second half of the group was used to test for potential infiltration of macrophages by comparing T2 maps recorded prior and 24 h following intravenous (i.v.) USPIO administration (Sinerem®, Laboratoires Guerbet, Roissy, France) at a dose of 340 μmol Fe/kg (injection volume: 2 ml/kg). USPIOs were administered immediately after the first T2 measurement (pre-USPIO). Post-USPIO T2 values were recorded at day 3, 10 and 38 following TAM. The elimination half-life of the USPIO used is approximately 5 h (Dousset et al., 1999b) and the time, during which USPIO-labeled macrophages remain visible in MR images, is of the order of 2–3 days

post-injection (Rausch et al., 2001). With an interval of 7 days between injections, the MR signal of subsequent measurements was not or only minimally affected by USPIOs administered during the previous imaging session. For the acquisition of DTI maps four treated (+TAM) and two littermate control mice (–TAM) were used. DTI experiments were carried out at day 3, 8 and 11 (baseline) and at day 35 and 39 (end stage) after start of TAM injections.

2.6 Image analysis

T2 and MTR maps were calculated using Biomap (M. Rausch, Novartis, Switzerland) with T2 derived from single-exponential fitting and MTR calculated as MTR(%) = (MS/M0)×100, with M0 and Ms representing the signal magnitude in the absence of a saturation pulse (control experiment) and the steady-state signal magnitude during MT saturation, respectively. Calculations of the invariant DTI-based parametric maps, performed on a voxel-by-voxel basis, were done using an in-house software routine written in IDL (RSI, Boulder, USA). Diffusion-weighted images were processed to generate the six independent elements of the diffusion tensor *D*. A real eigenvalue decomposition of the symmetric tensor *D* yielded the orthonormal eigenvectors e*i* (i=1,2,3) and the diagonal matrix comprising the eigenvalues ($\lambda1$, $\lambda2$ and $\lambda3$). Quantitative invariant indices, such as axial diffusivity ($\lambda\|=\lambda1$), radial diffusivity ($\lambda\perp=(\lambda2+\lambda3)/2$) and fractional anisotropy (FA) were calculated according to Le Bihan et al (Le Bihan et al., 2001). FA is a measure of anisotropy of the water diffusion within a given voxel and by definition ranges between 0 (isotropic) and 1 (maximally anisotropic). Color-coded FA

maps were generated using ParaVision® Jive.

2.7 Co-registration and Statistical analysis

All calculated parasagittal T2 maps from the same individual were co-registered manually using affine transformation and T2 values for baseline (average of values of day 2 and 9) and end stage (average of values of day 37 and 41) for the defined ROIs (fx, frontal cortex; ob, olfactory bulb; cb, cerebellar white matter; bs, brainstem; Fig. 2). ΔT2 changes after USPIO administration in –TAM and +TAM mice were calculated as difference T2 (24 h post)-T2(pre) injection for baseline (average of day 3 and 10) and end stage (day 38). Computed MTR maps were re-sliced and co-registered manually to the high-resolution images using affine transformation. ROIs for quantitative analysis were defined on high-resolution images for fx, ob, cb and bs, and transposed onto MTR maps to derive values for baseline (average of values of day 2 and 9) and end stage (average of values of day 37 and 41). FA, axonal ($\lambda\parallel$) and radial diffusivity ($\lambda\perp$) were derived by performing anatomy-based ROI analysis with ROIs selected in cb and bs based on highresolution images. DTI parameters were derived for baseline time point (average values of day 3, 8 and 11) and end stage (average value of day 35 and 39). All data in text are given as mean ± SEM or plotted as box plot (main quartiles, sample minimum and maximum). Data were statistically analyzed using ANOVA and Fisher's PLSD posthoc test for single comparisons.

2.8 Histological analysis

Mice were directly post-scan transcardially perfused with heparin (250 mg/l PBS, Sigma-Aldrich, Steinheim, Germany) in phosphate buffered saline (PBS) followed by fixation with 4 % paraformaldehyde (Sigma-Aldrich, Steinheim, Germany). Brains were dissected, cut into halves, post-fixed and embedded in paraffin (Medite, Nunningen, Switzerland). Brains were sectioned into 5 µm coronal or sagittal sections and taken up on polysine glass slides (Menzel, Braunschweig, Germany). Luxol-Fast-Blue (LFB) and Luxol-Nissl (L-N) stainings were executed according to standard procedures. In short, sections were deparaffinized, rehydrated to 95 % alcohol, heated in 0.1 % LFB (Sigma-Aldrich, Steinheim, Germany) in a microwave, differentiated with 0.05 % lithium carbonate (Sigma-Aldrich, Steinheim, Germany) and alcohol and for L-N counterstained with cresyl violet acetate (Sigma-Aldrich, Steinheim, Germany).

Prussian blue staining for iron was executed according to standard procedures. In short, sections were deparaffinized, rehydrated, stained for iron with potassium ferrocyanide trihydrate in hydrochloric acid solution and counterstained with nuclear fast red (all Sigma-Aldrich, Steinheim, Germany).

For immunohistochemistry, sections were deparaffinized, rehydrated and exposed to heat-mediated antigen retrieval using a tissue microwave oven (Medite, Nunningen, Switzerland). Endogenous peroxidase was blocked with 3 % H2O2/methanol (Sigma-Aldrich, Steinheim, Germany), followed by blocking and permeabilisation with blocking buffer (10 % fetal calf serum (Brunschwig, Basel, Switzerland), 1 % bovine serum albumine and 0.1 % Triton X-100 (both Sigma-Aldrich, Steinheim,

Germany) in PBS) and primary antibody (mouse-anti-CNPase (1:100; Sigma-Aldrich, Steinheim, Germany)) was incubated over night at 4°C in blocking buffer. Sections were washed, incubated with corresponding biotinylated secondary antibodies (1:500; JacksonImmunoResearch, Suffolk, United Kingdom) followed by incubation with Vectastain® ABC reagent mix (Reactolab, Servion, Switzerland) and developed with DAB metal enhancer solution (Thermo Scientific, Waltham, United States). Sections were documented using a Zeiss AxioImager Microscope and an AxioCam MRc5 (Zeiss, Goettingen, Germany). Image Processing was performed using Zeiss Axiocam (Zeiss, Goettingen, Germany) and Photoshop (Adobe Systems Incorporated, California, United States).

For semi- and ultrathin resin sectioning, tissues were postfixed and contrasted with 2 % osmium tetroxide (EMS, Hatfield, USA), dehydrated with acetone, embedded in corrected Spurr's resin (EMS, Hatfield, USA) (Ellis, 2006), sectioned into 0.5 µm or 80 nm sections using a fine microtome (Ultracut E, Leica, Wetzlar, Germany) and taken up on standard glass slides (Menzel, Braunschweig, Germany) or copper EM grids (EMS, Hatfield, USA). Semithin sections for light microscopy were contrasted with 1 % tolluidine blue (Sigma-Aldrich, Steinheim, Germany) and ultrathin sections for electron microscopy with 3 % uranyl acetate and 1 % lead citrate.

3. Results

To test for effects of temporally and spatially controlled oligodendrocyte cell death we quantitatively assessed in individual animals intrinsic T2 values, T2 changes caused by infiltration of USPIO labeled monocytes, MTR and anisotropic water diffusion in diseased animals (+TAM) at baseline before the occurrence of clinical signs (<day 15 after first injection of tamoxifen), referring to score 0 based on clinical scoring, and at end stage pathology (>day 35), referring to score 2-3. Control littermates (-TAM) underwent imaging at the same time points after injection of vehicle.

3.1 Increased T2 - *values in cerebellum and brainstem of diseased +TAM mice*

T2 maps of +TAM mice at end stage revealed distinct areas of pronounced hyperintensities in brainstem and cerebellum, regions known to be strongly affected by intrinsically triggered oligodendrocyte cell death (Pohl et al., 2011). Parasagittal T2 maps 0.4 mm lateral relative to Bregma of representative animals from -TAM or +TAM at day 2 and 41, were compared to corresponding Luxol-Nissl (L-N) stained histological sections of day 41. For +TAM mice a pronounced reduction in myelin in brainstem and cerebellum was found (Fig. 1). Hyperintense areas visible on T2 maps matched regions of cerebellar white matter and brain stem damage on histological sections stained with L-N, which appeared as less stained, vacuolized, widespread structures (visible on L-N sections). Quantitative analysis of T2 values derived from ROIs revealed identical values for both the +TAM and –TAM group at baseline (Fig. 2). At end stage of the disease process animals from +TAM group

show significantly increased T2 values compared to -TAM in brainstem (ΔT2 = 8.8 ± 1.5 ms, p < 0.001; Fisher's PLSD posthoc test) and cerebellum ROI (ΔT2 = 9.97 ± 1.8 ms, p < 0.001) or when compared to both –TAM animals or +TAM mice before disease onset (for brainstem ΔT2 = 9.84 ± 1.3 ms p < 0.001, for cerebellum ΔT2 = 13.5 ± 1.5 ms, p < 0.001). No other age and trait related differences were observed except in the frontal cortex, where we measured slightly decreased T2 values in end stage +TAM animals compared to +TAM mice at baseline acquisition (ΔT2 = -1.0 ± 0.4 ms, p = 0.032) or to –TAM at end stage (ΔT2= -1.2 ± 0.5 ms, p = 0.04).

3.2 Absence of monocyte infiltration in affected brain structures of diseased +TAM mice

To test for potential infiltration of blood-borne monocytes we assessed ΔT2 values 24 h after systemic injection of USPIO at a concentration of 340 µmol Fe/kg. Quantitative analysis of changes in T2 calculated as ΔT2 = T2(24 h post) - T2(pre) injection (Table 1) revealed no significant difference related to age and trait for brainstem (overall ANOVA; F(3, 11) F=0.56, p = 0.65), and for the two control regions in the olfactory bulb (F=1.3, p = 0.35) and frontal cortex (F=1.05, p = 0.42). In the cerebellum we found a significant, albeit small difference between –TAM and +TAM animals at baseline (Fisher; p = 0.035), but not at end stage (p = 0.866). Prussian blue staining, specific for ferric iron, of corresponding tissue sections confirmed the absence of iron within the regions affected by oligodendrocyte cell death in the cerebellum (Suppl. Fig. 1). Only very few single Prussian blue positive cells have been detected (1-3 cells per brain section), which were mostly associated with vessels in -TAM and +TAM mice at end stage (day 38). In contrast, Prussian blue staining of liver sections of a naïve (untreated) animal 24 h after injection of USPIO (+USPIO) as a control showed strong accumulation of cell associated iron compared to injection of vehicle (-USPIO).

3.3 Reduction of diffusional anisotropy in brainstem and cerebellum of diseased +TAM animals

From DTI, values for fractional anisotropy (FA), axonal ($\lambda\parallel$) and radial diffusivity ($\lambda\perp$) were calculated. Figure 3 shows coronal T2-weighted MRI section at the level of -2.3 mm relative to Bregma with superimposed ROIs in cerebellar white matter and in the brainstem used for the analysis of diffusion parameters, the corresponding diffusion direction-dependent color-coded FA maps and histological sections for representative animals from –TAM and +TAM group at day 39 (end stage). The color-coded FA maps revealed pronounced abnormalities in +TAM animals at end stage, which spatially matched structures affected by demyelination indicated by as loss of myelin on corresponding histological sections stained for myelin content (LFB, CNPase) (Fig. 3, indicated by arrows). FA values of +TAM mice were significantly decreased in brainstem (overall ANOVA; F(3, 11) F = 4.24, p = 0.045; Fig. 4) and cerebellum (F(3, 11) F=14.97, p = 0.001; Fig. 4), and when compared to -TAM animals at end stage (bs: p = 0.043; cb: p = 0.0006) or to +TAM at baseline (bs: p = 0.019; cb: p = 0.0005). Regarding directional diffusion coefficients, the analyses revealed a

significant decrease in $\lambda_{\parallel}$ in diseased mice for brainstem (overall ANOVA, F(3, 11) F = 10.58, p = 0.004) and cerebellum (F(3, 11) F = 22.21, p = 0.0003), and when compared to control at end stage (bs: p = 0.021; cb: p = 0.0015) or to +TAM at baseline (bs: p = 0.0097; cb: p = 0.00006). For both regions analyzed, no significant difference between +TAM and –TAM mice was found for radial diffusivity, although in the brainstem a trend of an increased $\lambda_{\perp}$ in +TAM mice at end stage was observed when compared to the baseline stage (Fig. 4, p = 0.056).

3.4 Decreased MTR values in brainstem of diseased +TAM mice.

Qualitative analysis of color-coded MTR maps (Fig. 5) at the level of -2.3 mm relative to the Bregma of representative animals from –TAM and +TAM at baseline acquisition (day 3) and end stage (day 40) indicated a decrease in MTR values in affected areas (brainstem) for end stage +TAM mice. An average MTR value of brain tissue of the order of 50-55 % was found, which was slightly decreased in the brainstem ROI of +TAM when compared to -TAM mice at day 40. Variance analysis of MTR values (Table 2) revealed significant group differences for the brainstem ROI (F(3, 11) F = 3.55, p = 0.05) between baseline and end stage +TAM mice (p=0.027) and between -TAM and +TAM at end stage (p = 0.038). No significant differences were observed in MTR values in cerebellar white matter (F(3,11) F = 1.49, p = 0.289). Similarly no difference in MTR between –TAM and +TAM animals was found in control ROI in the olfactory bulb or in the frontal cortex (derived from MTR sections at the level of +8 mm or +5 mm relative to the Bregma, respectively (ROIs and MTR maps not shown)).

4. Discussion

Experimentally, demyelination as occurring in MS and its histopathological and functional consequences are widely studied as part of the pathological cascade triggered by a primary inflammatory process in rat and mouse EAE. Application of T2 weighted MRI in such models typically revealed hyperintense lesions on T2-weighted images corresponding to regions of edema formation. Sites of BBB breakdown detected by Gd-DTPA enhanced MRI were in general found to correlate with areas of macrophage recruitment (Nessler et al., 2007; Serres et al., 2009). Detection of areas displaying neuronal damage such as myelin loss is commonly compromised by this dominating MRI signature attributed to inflammatory processes.

In the novel mouse model investigated in this study, cell death of myelinating oligodendrocytes is intrinsically triggered and can be spatially and temporally controlled (Pohl et al., 2011), which allows studying neurodegenerative processes potentially involved in MS independent of inflammatory processes. This model results in an ablation of approximately 80 % of cells throughout the oligodendroglial lineage within a few days and produces a consistent disease course. The model is essentially devoid of a peripheral immunological component and myelin damage occurs

predominantly in spatially confined areas of cerebellar white matter and brainstem. Interestingly, T2 maps of severely affected mice displayed pronounced T2 increases within white matter tracts, as confirmed by histopathological analysis: for cerebellar white matter the regions of increased T2 values matched areas of demyelination visualized as vacuolated structures on L-N stained histological sections. The occurrence of discrete hyper-intense lesions on T2 -weighted images is considered an MRI hallmark of MS (Fazekas et al., 1999). Such T2 hyper-intensities are mainly reflecting an inflammatory response with other pathological processes such as demyelination, axonal loss and gliosis (Bruck et al., 1997; van Walderveen et al., 1998; van Waesberghe et al., 1999) contributing to the signal changes.

In the model described, we did not observe any hypo-intense areas in cerebellum or brainstem. In MS patients, hypo-intense signals on T2-weighted images have been described at the border of early active lesions in patients (Landtblom et al., 1996; Bruck et al., 1997) and MS-like lesions in EAE models (Broom et al., 2005) and found to correlate with actively phagocyting macrophages and/or the density of reactive astrocytes. Reduced T2 values have been associated with partial necrosis or high cellularity as observed in proliferative tissue (Carrier et al., 1994; Koeller et al., 1997). In a T-cell-clone-mediated mouse model of MS, Nessler et al. (Nessler et al., 2007) described lesion types characterized by a hypo-intense lesion core, for which the signal intensity in T2 weighted images showed a stronger correlation with the density of activated microglia cells than with reactive astrocytes. Taken together, there is strong evidence that hypo-intense areas on T2 -weighted images at the core or rim of early MS lesion reflect pronounced hypercellularity caused by infiltrating macrophages and/or activated microglia cells. The absence of T2 hypo-intensities in cerebellum or brainstem in this model of oligodendrogliopathy may therefore be attributed to its negligible inflammatory component. Consistent with this interpretation, USPIO-enhanced MRI, a method for monitoring the infiltration of blood-borne macrophages (Dousset et al., 1999a; Rausch et al., 2003; Floris et al., 2004; Berger et al., 2006; Brochert et al., 2006; Ladewig et al., 2009) did not reveal areas of signal decreases in +TAM mice at any time point, reflecting very weak recruitment of blood-borne immune cells in this intrinsically triggered model of glial cell ablation.

The decreased FA values observed in end stage +TAM mice as compared to –TAM animals are indicative of white matter disease in cerebellum and brainstem, the areas strongest affected by the intrinsic ablation of oligodendrocytes. Although being exquisitely sensitive to the pathological process affecting white matter, anisotropy is not specific to either axonal damage or demyelination. Analysis of directional diffusion coefficients is needed for discrimination of axonal damage associated with a decrease in the water diffusion parallel to the white matter fibers ($\lambda_{\parallel}$), and/or demyelination suggested to be reflected by an increase in the radial diffusion coefficient ($\lambda_{\perp}$). In the present mouse model we observed a pronounced decrease in axial diffusivity at end stage in both brainstem and cerebellum white matter structures. It has been shown that axial diffusivity is highly correlated with axonal damage in EAE mice (DeBoy et al., 2007; Budde et al., 2008) and mouse models of other white matter

injuries (Sun et al., 2006; Kim et al., 2007; Mac Donald et al., 2007) resulting from the loss of coherent organization of the axon. Decreased axial diffusivity has been associated with axonal swelling (Song et al. 2005), Wallerian degeneration (Song et al. 2003), diffuse axonal injury (Arfanakis et al. 2002) or axonal integrity/neurofilament dysfunction (positive SMI-32 staining) (Budde et al., 2009; Sun et al. 2006). We attribute the strongly reduced $\lambda\parallel$ values to axonal damage, which has been demonstrated by marker analysis for axonal impairment and disorganization, as well as morphological findings typical for axonal defects (Pohl et al., 2011) in regions affected by oligodendrocyte cell death.

In the regions strongest affected by the consequences of oligodendroglial ablation, we did not observe a significant difference in radial diffusivity $\lambda\perp$ between +TAM and –TAM mice at end stage pathology, which at a first glance seems contradictory to expectations for a model of specific and intrinsically triggered oligodendrocyte cell death. There are, however, several factors which may account for the absence of an increased radial diffusivity. Technical aspects include partial volume effects that might reduce the sensitivity of DTI in detecting effects due to demyelination. In voxels not entirely confined to white matter such as the region selected for brainstem, contributions of compartments characterized by different FA values within a given region-of-interest will reduce the sensitivity for detecting changes as the directional diffusivities. Nevertheless, the mean anisotropy values of 0.41 and 0.58 as measured in brainstem and cerebellum of -TAM mice, respectively, are indicative of a predominant contribution of white matter fibers possessing a uniform orientation. Substantial amount of remaining myelin debris and semi-intact myelin sheaths might alleviate the effects on diffusion perpendicular to the axon rendering them too small to significantly alter $\lambda\perp$. Additionally, microglia and astrocytic protrusions filling the space previously occupied by myelin might provide diffusion barriers counteracting the possible effect by the loss of myelin membranes.

Finally, axonal shrinkage as well as remyelination might counteract increases in lateral diffusion. Both in cerebellum and brainstem the radial diffusivity in +TAM at end stage tended to be higher compared to -TAM mice, albeit the difference did not reach the significance level. Assessing directional diffusivity in demyelinated lesions, which lack an inflammatory component, is an attractive tool to disentangle the paradox situation existing when interpreting MRI findings inherently present in EAE models. Although the presence of altered radial diffusivity has been shown in several demyelinating models (Song et al., 2005), radial diffusivity may not be as specific in the presence of other pathological changes. For instance, it has not been well defined whether radial diffusivity is specific to demyelination in the presence of significant inflammation. To what extend the absence of an inflammatory component in model described can be accounted for the small changes in radial diffusivity has to be further explored.

Despite the absence of a clear-cut effect on radial diffusivity the significant decreases in MTR observed in the brainstem of diseased mice at late stage in the pathology is assumed to reflect the loss of myelin and its integrity, the predominant macromolecular structure rich in protons in white matter.

MTR has been suggested to represent predominantly a measure of myelin integrity (Schmierer et al., 2004). The relatively weak and heterogeneous changes in MTR observed in cerebellar structures in our model might be in part explained by the myelin debris residing in these structures at end stage (Pohl et al., 2011). Nevertheless, there is substantial damage or loss of myelin in brainstem areas sufficient to translate into a clear reduction in MTR. Interestingly in this context are recent findings in two different EAE models that early MTR decreases preceded the onset of demyelination (Serres et al., 2009). The studies confirm previous reports stating that MTR changes more closely reflect inflammatory events, i.e. dilution of macromolecules as a consequence of edema formation, than myelin loss (Gareau et al., 2000). It has therefore been suggested that MTR changes in MS may reflect events leading to demyelination rather than demyelination *per se*.

5. Conclusion

We evaluated the sensitivity of various MRI methods to detect histopathological changes in mice after loss of myelinating glia. This novel mouse model based on spatially and temporally controlled oligodendrocyte cell ablation allowed studying the MRI signature associated to neurodegenerative processes related to MS in the absence of the autoimmune components that appear to be foremost in EAE models. Pronounced T2 hyperintensities matched the regional distribution of cell ablation in cerebellar and brainstem white matter as revealed by histology with affected regions being devoid of significant macrophage infiltration. Elevated T2 values that are commonly associated to the inflammatory response have been attributed to structural remodeling of white matter structures involving pronounced vacuolation. The significant decrease in diffusion anisotropy derived from DTI measures in these structures is mainly caused by a pronounced decrease in diffusivity parallel to the fiber indicative of axonal damage. Triggering of oligodendrocyte ablation did not translate into a significant increase in radial diffusivity; similarly, only minor decreases in MTR have been observed. It remains unclear to what extend these latter findings are due to myelin debris remaining in the tissue. Alternatively, it could indicate that in EAE models both radial diffusivity and MTR are significantly influenced by the strong initial and persistent inflammatory component. Models, such as the oligodendrocyte ablation model described, lacking the strong inflammatory component dominating the MRI signatures, should be of value in identifying potential biomarkers of MS that are characteristic for neurodegenerative aspects of the disease.

Acknowledgements

This work was supported by the Swiss National Science Foundation and the National Center for Competence in Research (NCCR) Neural Plasticity and Repair. We thank the Light Microscopy Center of the ETH Zurich, Switzerland, for excellent support.

References

Arfanakis, K., Hermann, B., Rogers, B.P., Carew, J.D., Seidenberg, M., Meyerand, M.E., 2002. Diffusion tensor MRI in temporal lobe epilepsy. Magn. Reson. Imaging 20, 511-519.

Bakshi, R., Thompson, A.J., Rocca, M.A., Pelletier, D., Dousset, V., Barkhof, F., Inglese, M., Guttmann, C.R.G., Horsfield, M.A., Filippi, M., 2008. MRI in multiple sclerosis: current status and future prospects. Lancet Neurol. 7, 615-625.

Barkhof, F., 2002. The clinico-radiological paradox in multiple sclerosis revisited. Curr. Opin. Neurol. 15, 239-245.

Barnett, M.H., Prineas, J.W., 2004. Relapsing and remitting multiple sclerosis: Pathology of the newly forming lesion. Ann. Neurol. 55, 458-468.

Basser, P.J., Mattiello, J., Lebihan, D., 1994. MR Diffusion Tensor Spectroscopy and Imaging. Biophys. J. 66, 259-267.

Berger, C., Hiestand, P., Kindler-Baumann, D., Rudin, M., Rausch, M., 2006. Analysis of lesion development during acute inflammation and remission in a rat model of experimental autoimmune encephalomyelitis by visualization of macrophage infiltration, demyelination and blood-brain barrier damage. NMR in Biomed. 19, 101-107.

Brochet, B., Deloire, M.S.A., Touil, T., Anne, O., Caille, J.M., Dousset, V., Petry, K.G., 2006. Early macrophage MRI of inflammatory lesions predicts lesion severity and disease development in relapsing EAE. NeuroImage 32, 266-274.

Brockschnieder, D., Lappe-Siefke, C., Goebbels, S., Boesl, M.R., Nave, K.A., Riethmacher, D., 2004. Cell depletion due to diphtheria toxin fragment A after Cre mediated recombination. Mol. Cell. Biol. 24, 7636-7642.

Broom, K.A., Anthony, D.C., Blamire, A.M., Waters, S., Styles, P., Perry, V.H., Sibson, N.R., 2005. MRI reveals that early changes in cerebral blood volume precede blood brain barrier breakdown and overt pathology in MS-like lesions in rat brain. J. Cereb.Blood Flow Metab. 25, 204-216.

Bruck, W., Bitsch, A., Kolenda, H., Bruck, Y., Stiefel, M., Lassmann, H., 1997. Inflammatory central nervous system demyelination: Correlation of magnetic resonance imaging findings with lesion pathology. Ann. Neurol. 42, 783-793.

Budde, M., Kim, J., Liang, H., Russell, J.H., Cross, A.H., Song, S., 2008. Axonal injury detected by in vivo diffusion tensor imaging correlates with neurological disability in a mouse model of multiple sclerosis. NMR Biomed. 21, 589-597.

Budde, M.D., Xie, M., Cross, A.H., Song, S.-K., 2009. Axial Diffusivity Is the Primary Correlate of Axonal Injury in the Experimental Autoimmune Encephalomyelitis Spinal Cord: A Quantitative Pixelwise Analysis. J. Neurosci. 29, 2805-2813.

Carrier, D.A., Mawad, M.E., Kirkpatrick, J.B., Schmid, M.F., 1994. Metastatic Adenocarcinoma to the Brain - MR with Pathological Correlation. AJNR Am. J. Neuroradiol. 15, 155-159.

Deboy, C.A., Zhang, J., Dike, S., Shats, I., Jones, M., Reich, D.S., Mori, S., Nguyen, T., Rothstein, B., Miller, R.H., Griffin, J.T., Kerr, D.A., Calabresi, P.A., 2007. High resolution diffusion tensor imaging of axonal damage in focal inflammatory and demyelinating lesions in rat spinal cord. Brain 130, 2199-2210.

Dousset, V., Delalande, C., Ballarino, L., Quesson, B., Seilhan, D., Coussemacq, M., Thiaudiere, E., Brochet, B., Canioni, P., Caille, J.M., 1999a. In vivo macrophage activity imaging in the central nervous system detected by magnetic resonance. Magn.Reson.Med. 41, 329.

Dousset, V., Gomez, C., Petry, K.G., Delalande, C., Caille, J.M., 1999b. Dose and scanning delay using USPIO for central nervous system macrophage imaging. Magma 8, 185-189.

Ellis, E., 2006. Corrected formulation for Spurr low viscosity embedding medium using the replacement epoxide ERL 4221. Microsc. Microanal. 12, 288–289.

Fazekas, F., Barkhof, F., Filippi, M., Grossman, R.I., Li, D.K.B., McDonald, W.I., McFarland, H.F., Paty, D.W., Simon, J.H., Wolinsky, J.S., Miller, D.H., 1999. The contribution of magnetic resonance imaging to the diagnosis of multiple sclerosis. Neurology 53, 448-456.

Filippi, M., Agosta, F., 2009. Magnetic resonance techniques to quantify tissue damage, tissue repair, and functional cortical reorganization in multiple sclerosis. Prog. Brain Res. 175, 465-482.

Floris, S., Blezer, E.L.A., Schreibelt, G., Dopp, E., van der Pol, S.M.A., Schadee-Eestermans, I.L., Nicolay, K., Dijkstra, C.D., de Vries, H.E., 2004. Blood-brain barrier permeability and monocyte infiltration in experimental allergic encephalomyelitis - A quantitative MRI study. Brain 127, 616-627.

Frohman, E.M., Racke, M.K., Raine, C.S., 2006. Multiple Sclerosis -- The Plaque and Its Pathogenesis. N. Engl. J. Med. 354, 942-955.

Gareau, P.J., Rutt, B.K., Karlik, S.J., Mitchell, J.R., 2000. Magnetization transfer and multicomponent T2 relaxation measurements with histopathologic correlation in an experimental model of MS. J. Magn. Reson. Imaging 11, 586-595.

Hennig, J., Nauerth, A., Friedburg, H., 1986. RARE imaging: a fast imaging method for clinical MR. Magn. Reson. Med. 3, 823-833.

Kim, J.H., Loy, D.N., Liang, H.F., Trinkaus, K., Schmidt, R.E., Song, S.K., 2007. Noninvasive diffusion tensor imaging of evolving white matter pathology in a mouse model of acute spinal cord injury. Magn. Reson. Med. 58, 253-260.

Koeller, K.K., Smirniotopoulos, J.G., Jones, R.V., 1997. From the archives of the AFIP - Primary central nervous system lymphoma: Radiologic-pathologic correlation. Radiographics 17, 1497-1526.

Ladewig, G., Jestaedt, L., Misselwitz, B., Solymosi, L., Toyka, K., Bendszus, M., Stoll, G., 2009. Spatial diversity of blood-brain barrier alteration and macrophage invasion in experimental autoimmune encephalomyelitis: A comparative MRI study. Exp.Neurol. 220, 207-211.

Landtblom, A.M., Sjoqvist, L., Soderfeldt, B., Nyland, H., Thuomas, K.A., 1996. Proton MR spectroscopy and MR imaging in acute and chronic multiple sclerosis – Ringlike appearances in acute plaques. Acta radiol. 37, 278-287.

Lassmann, H., 2008. Models of multiple sclerosis: new insights into pathophysiology and repair. Curr. Opin. Neurol. 21, 242-247.

Lassmann H., 2005. Multiple sclerosis pathology: evolution of pathogenetic concepts. Brain Pathol. 15, 217-22.

Lassmann, H., Brück, W., Lucchinetti, C., 2001. Heterogeneity of multiple sclerosis pathogenesis: implications for diagnosis and therapy. Trends Mol. Med. 7, 115-121.

Le Bihan, D., Mangin, J.F., Poupon, C., Clark, C.A., Pappata, S., Molko, N., Chabriat, H., 2001. Diffusion tensor imaging: Concepts and applications. J. Magn. Reson.Imaging 13, 534-546.

Leist, T.P., Marks, S., 2010. Magnetic resonance imaging and treatment effects of multiple sclerosis therapeutics. Neurology 74, S54-S61.

Leone, D.P., Genoud, S., Atanasoski, S., Grausenburger, R., Berger, P., Metzger, D., Macklin, W.B., Chambon, P., Suter, U., 2003. Tamoxifen-inducible glia-specific Cre mice for somatic mutagenesis in oligodendrocytes and Schwann cells. Mol. Cell. Neurosci. 22, 430-440.

Ludwin, S.K., 2006. The Pathogenesis of Multiple Sclerosis: Relating Human Pathology to Experimental Studies. J. Neuropathol. Exp. Neurol. 65, 305-318.

Mac Donald, C.L., Dikranian, K., Bayly, P., Holtzman, D., Brody, D., 2007. Diffusion tensor imaging reliably detects experimental traumatic axonal injury and indicates approximate time of injury. J. Neurosci. 27, 11869-11876.

Matthaei, I., Polman, C.H., de Groot, C.J., Dijkstra, C.D., Koetsier, J.C., and Sminia, T., 1989. Observer agreement in the assessment of clinical signs in experimental allergic encephalomyelitis. J. Neuroimmunol. 23, 25-28.

Nessler, S., Boretius, S., Stadelmann, C., Bittner, A., Merkler, D., Hartung, H.P., Michaelis, T., Bruck, W., Frahm, J., Sommer, N., Hemmer, B., 2007. Early MRI changes in a mouse model of multiple sclerosis are predictive of severe inflammatory tissue damage. Brain 130, 2186-2198.

Patrikios, P., Stadelmann, C., Kutzelnigg, A., Rauschka, H., Schmidbauer, M., Laursen, H., Sorensen, P.S., Bruck, W., Lucchinetti, C., Lassmann, H., 2006. Remyelination is extensive in a subset of multiple sclerosis patients. Brain 129, 3165-3172.

Pohl HB, Porcheri C, Mueggler T, Bachmann LC, Martino G, Riethmacher D, Franklin RJ, Rudin M, Suter U., 2011. Genetically induced adult oligodendrocyte cell death is associated with poor myelin clearance, reduced remyelination, and axonal damage. J.Neurosci. 31, 1069-80.

Prineas, J.W., Kwon, E.E., Cho, E.S., Sharer, L.R., 1984. Continual Breakdown and Regeneration of Myelin in Progressive Multiple-Sclerosis Plaques. Ann. N. Y. Acad. Sci. 436, 11-32.

Ratering, D., Baltes, C., Nordmeyer-Massner, J., Marek, D., Rudin, M., 2008. Performance of a 200-MHz cryogenic RF probe designed for MRI and MRS of the murine brain. Magn. Reson. Med. 59, 1440-1447.

Rausch, M., Hiestand, P., Baumann, D., Cannet, C., Rudin, M., 2003. MRI-based monitoring of inflammation and tissue damage in acute and chronic relapsing EAE. Magn. Reson. Med. 50, 309-314.

Rausch, M., Sauter, A., Frohlich, J., Neubacher, U., Radu, E.W., Rudin, M., 2001. Dynamic patterns of USPIO enhancement can be observed in macrophages after ischemic brain damage. Magn. Reson. Med. 46, 1018-1022.

Rausch, M., Tofts, P.S., Lervik, P., Walmsley, A.R., Mir, A., Schubart, A., Seabrook, T., 2009. Characterization of white matter damage in animal models of multiple sclerosis by magnetization transfer ratio and quantitative mapping of the apparent bound proton fraction f*. Mult. Scler. 15, 16-27.

Schmierer, K., Scaravilli, F., Altmann, D.R., Barker, G.J., Miller, D.H., 2004. Magnetization transfer ratio and myelin in postmortem multiple sclerosis brain. Ann. Neurol. 56, 407-415.

Serres, S., Anthony, D.C., Jiang, Y., Campbell, S.J., Broom, K.A., Khrapitchev, A., Sibson, N.R., 2009. Comparison of MRI signatures in pattern I and II multiple sclerosis models. NMR Biomed. 22, 1014-1024.

Song, S.K., Sun, S.W., Ju, W.K., Lin, S.J., Cross, A.H., Neufeld, A.H., 2003. Diffusion tensor imaging detects and differentiates axon and myelin degeneration in mouse optic nerve after retinal ischemia. NeuroImage 20, 1714-1722.

Song, S.K., Yoshino, J., Le, T.Q., Lin, S.J., Sun, S.W., Cross, A.H., Armstrong, R.C., 2005. Demyelination increases radial diffusivity in corpus callosum of mouse brain. NeuroImage 26, 132-140.

Sun, S.W., Liang, H.F., Trinkaus, K., Cross, A.H., Armstrong, R.C., Song, S.K., 2006. Noninvasive detection of cuprizone induced axonal damage and demyelination in the mouse corpus callosum. Magn. Reson. Med. 55, 302-308.

van Waesberghe, J., Kamphorst, W., De Groot, C.J.A., van Walderveen, M.A.A., Castelijns, J.A., Ravid, R., Nijeholt, G., van der Valk, P., Polman, C.H., Thompson, A.J., Barkhof, F., 1999. Axonal loss in multiple sclerosis lesions: Magnetic resonance imaging insights into substrates of disability. Ann. Neurol. 46, 747-754.

van Walderveen, M.A.A., Barkhof, F., Polman, C., Frequin, S., Hommes, O.R., Thompson, A.J., Valk, J., 1998. Patterns of brain magnetic resonance abnormalities on T-2-weighted spin echo images in clinical subgroups of multiple sclerosis: A large cross-sectional study. Eur. Neurol. 40, 91-98.

Whittall, K.P., MacKay, A.L., Graeb, D.A., Nugent, R.A., Li, D.K.B., Paty, D.W., 1997. In vivo measurement of T-2 distributions and water contents in normal human brain. Magn. Reson. Med. 37, 34-43.

Wolff, S.D., Balaban, R.S., 1989. Magnetization Transfer Contrast (Mtc) and Tissue Water Proton Relaxation Invivo. Magn. Reson. Med. 10, 135-144.

Zaaraoui, W., Deloire, M., Merle, M., Girard, C., Raffard, G., Biran, M., Inglese, M., Petry, K.G., Gonen, O., Brochet, B., Franconi, J.M., Dousset, V., 2008. Monitoring demyelination and remyelination by magnetization transfer imaging in the mouse brain at 9.4 T. MAGMA 21, 357-362.

Figure Legends

Figure 1. **(A)** Parasagittal, quantitative T2 maps and corresponding histological sections for representative animals at baseline (day 2) and end stage (day 41) after TAM-induced ablation of oligodendrocytes (+TAM) and controls (-TAM). Histological sections were Luxol-Nissl (L-N) stained for myelin content. **(B)** Magnifications from histological sections of end stage diseased animal are displayed for cerebellar regions. **(C)** ROIs in olfactory bulb (ob), frontal cortex (fx), brain stem (bs) and cerebellar white matter (cb) used for quantitative analysis of T2 relaxation times (Fig. 2) are shown on a parasagittal MRI section 0.4 mm lateral relative to the mid-sagittal plane.

Figure 2. Box plots of T2 values for –TAM and +TAM at baseline (day 2 and day 9) and end stage (day 37 and day 41) derived from ROIs (Fig. 1) in brainstem (bs), cerebellar core (cb), olfactory bulb (ob) and frontal cortex (fx). Data are given as median, sample minimum, sample maximum, 1st and 3rd quartiles. * = $p < 0.05$; **= $p < 0.01$.

Figure 3. **(A)** Diffusion direction-dependent color-coded FA maps and histological sections for representative animals from –TAM and +TAM group at day 39 (end stage). For the color-coded maps, red, blue, and green colors indicate structures aligning along left–right, anterior–posterior, and superior–inferior orientations, respectively. Corresponding histological sections were stained for myelin content using luxol fast blue (LFB) and antibodies for CNPase. **(B)** Toluidine blue contrasted resin section (left) and transmission electron micrograph (right) of cerebellar white matter. Indicated are typical morphological findings: myelin vacuolation (black arrowhead), disrupted myelin rings associated with axons (empty arrowhead), and axons showing signs of impairment and shrinkage (asterisk). **(C)** ROIs in cerebellar white matter (cb) and in the brainstem (bs) used for DTI parameter analysis (Fig. 4) are shown on the coronal T2-weighted MRI section at the level of -2.3 mm relative to Bregma.

Figure 4. Box plots of quantitative analysis of DTI parameters (FA: fractional anisotropy; $\lambda\parallel$: axonal diffusivity; $\lambda\perp$: radial diffusivity (perpendicular to main fiber orientation) for the ROIs in brainstem (A) and cerebellum white matter (B), respectively. Data are given as median, sample minimum, sample maximum and lower and upper quartiles. * = $p < 0.05$; **= $p < 0.01$ tested by ANOVA, Fisher's PLSD posthoc test.

Figure 5. **(A)** MTR maps (color-coded for percentage and superimposed on T2-weighted images) from representative animals for –TAM and +TAM group at day 2 (baseline) and day 41 (end stage). **(B)** ROIs in cerebellar white matter (cb) and brainstem (bs) used to quantify MT ratios (Table 1) are shown on the right panel superimposed on coronal T2-weighted MRI section at the level of -2.3 mm relative to Bregma.

Supplementary Figure 1. **(A)** Representative histological sagittal section at day 38 (corresponding to MRI T2 maps, Fig. 1) stained for iron (Prussian blue) and counterstained with nuclear fast red for –TAM and +TAM 24 h post USPIO injections. Magnified sections from cerebellar white matter (cb) show absence of pronounced iron staining in both –TAM and +TAM. **(B)** Prussian blue staining of liver sections (liver) of a naïve (untreated) animal 24 h after injection of USPIO (+USPIO) shows positive control for iron staining and exposure undetectable in vehicle-injected animals (-USPIO).

Table 1 – ΔT_2 values: T_2(24 h post) - T_2(pre) USPIO injection [ms]

time point	treatment	brainstem		cerebellar wm		olfactory bulb		frontal cx	
	TAM	mean	±SEM	mean	±SEM	mean	±SEM	mean	±SEM
baseline	-	0.235	0.325	0.925	0.097	0.144	0.139	0.861	0.327
	+	0.092	0.556	-0.644	0.567	0.397	0.199	-0.181	0.612
end stage	-	0.684	1.119	0.415	0.172	-0.425	0.216	-0.277	0.020
	+	1.049	0.530	0.307	0.114	-0.369	0.474	-0.747	0.583

Table 2 – MTR values

time point	treatment	brainstem		cerebellar wm		olfactory bulb		frontal cx	
	TAM	mean	±SEM	mean	±SEM	mean	±SEM	mean	±SEM
baseline	-	0.560	0.007	0.557	0.008	0.576	0.001	0.558	0.005
	+	0.558	0.010	0.539	0.013	0.572	0.003	0.567	0.005
end stage	-	0.562	0.009	0.553	0.004	0.576	0.005	0.571	0.006
	+	0.531	0.003	0.525	0.009	0.572	0.002	0.556	0.005

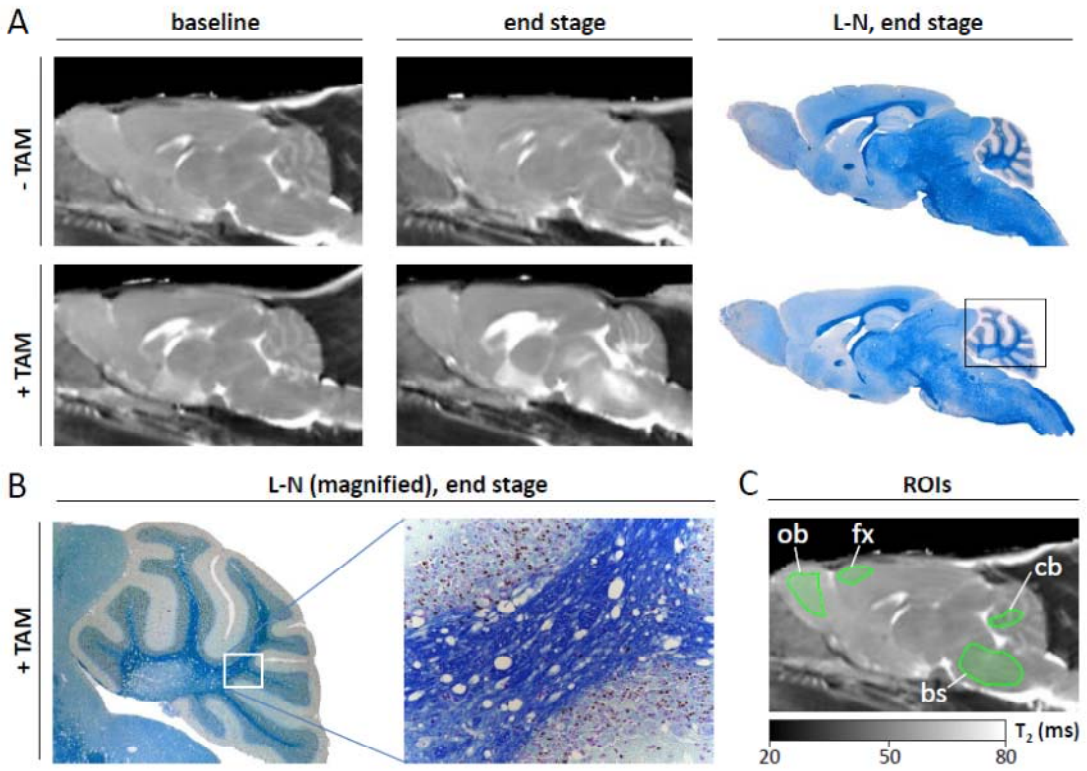

Figure 1

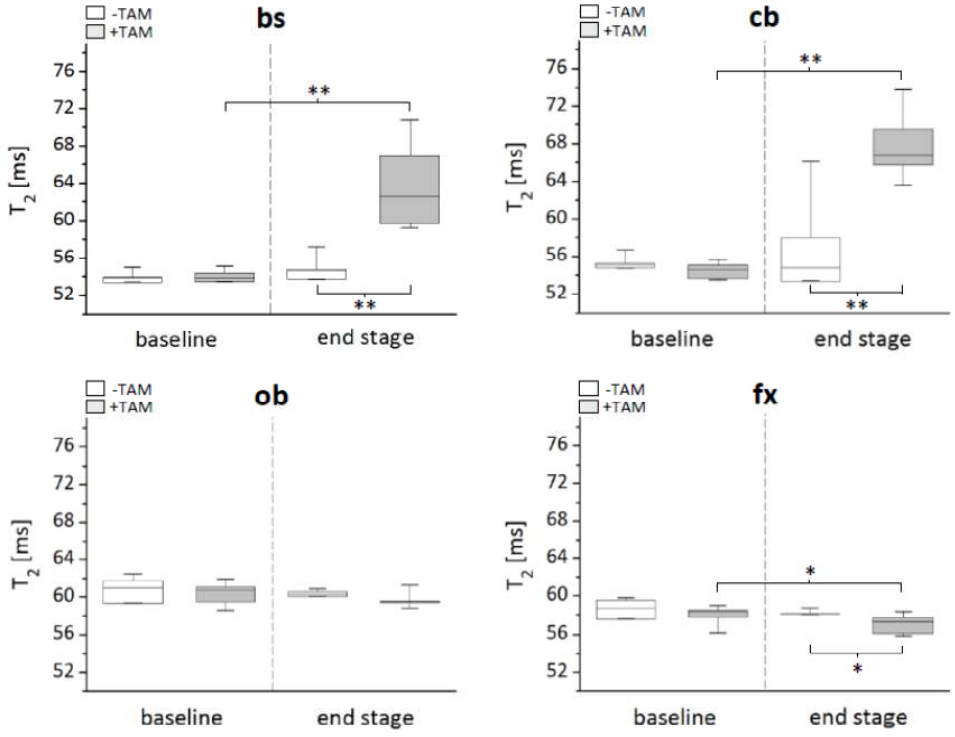

Figure 2

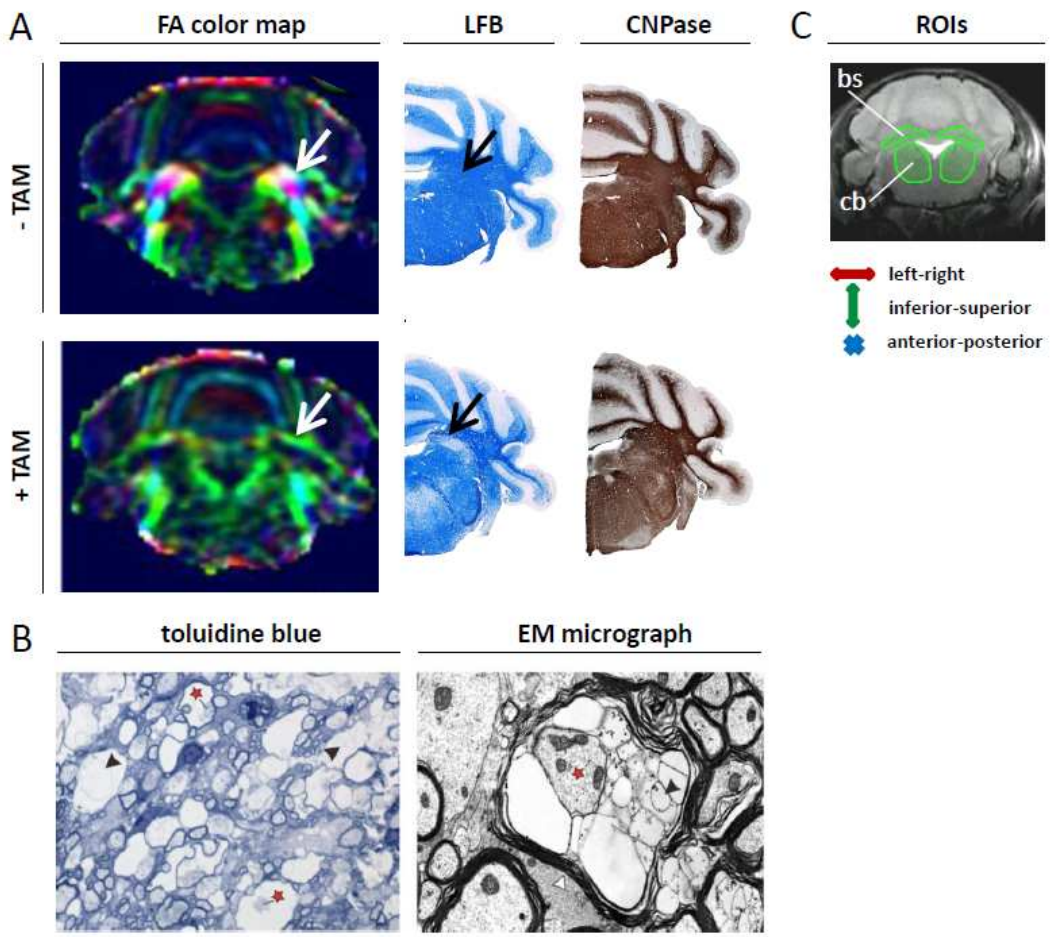

Figure 3

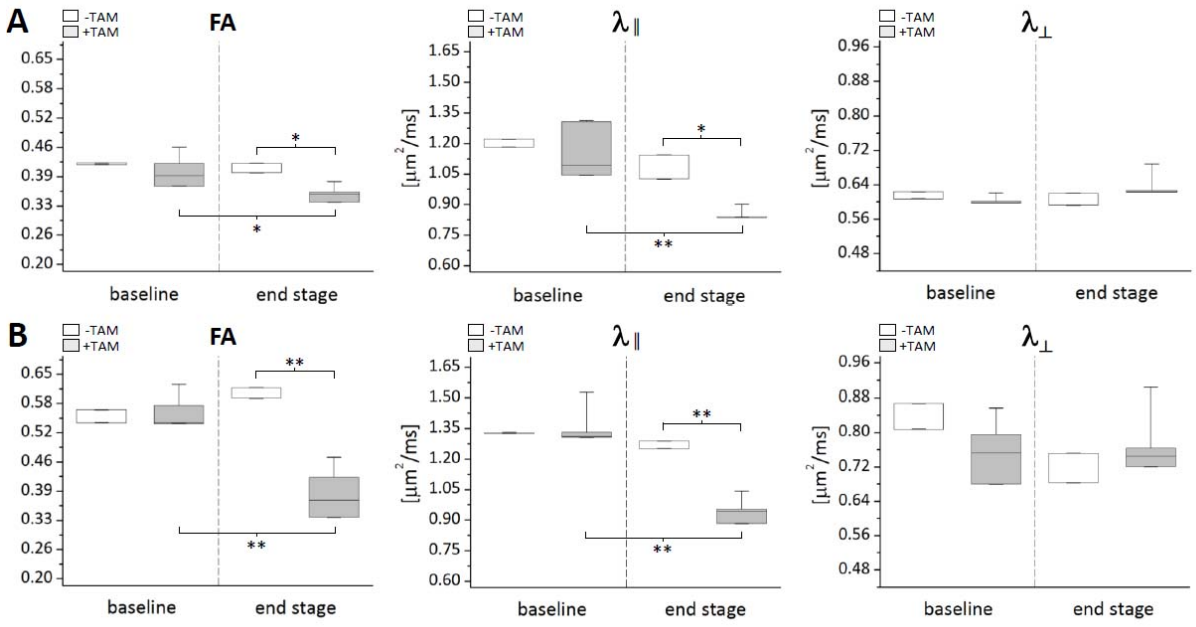

Figure 4

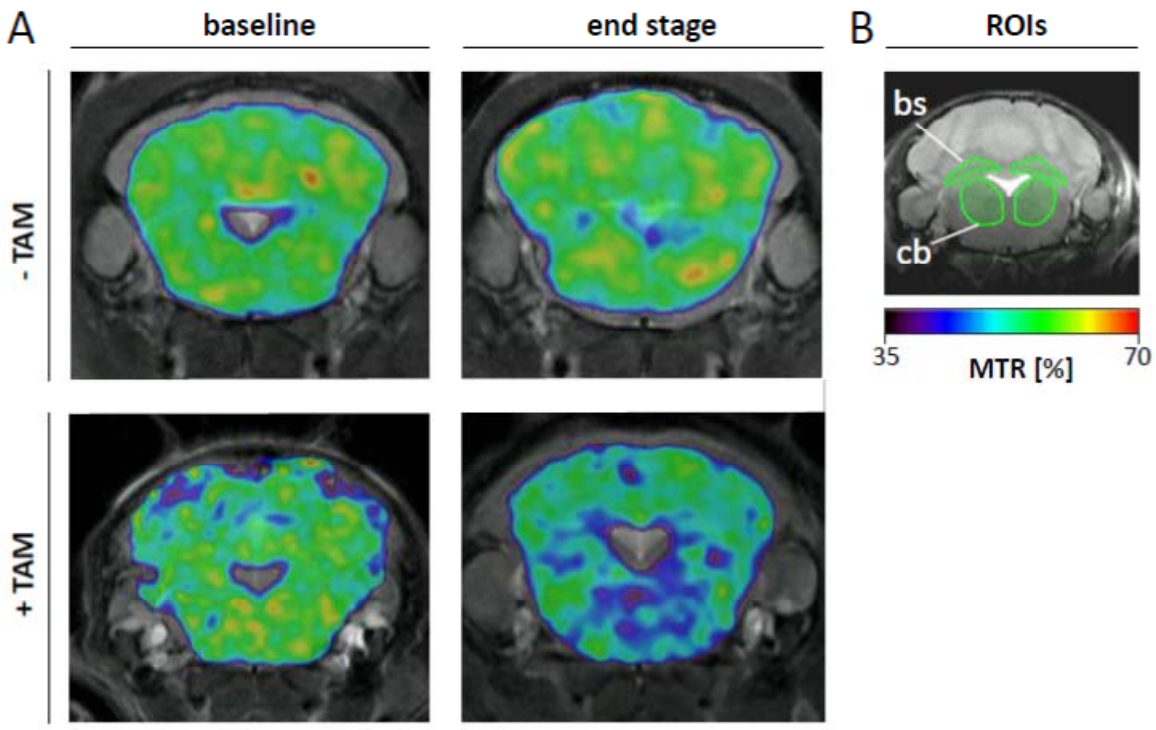

Figure 5

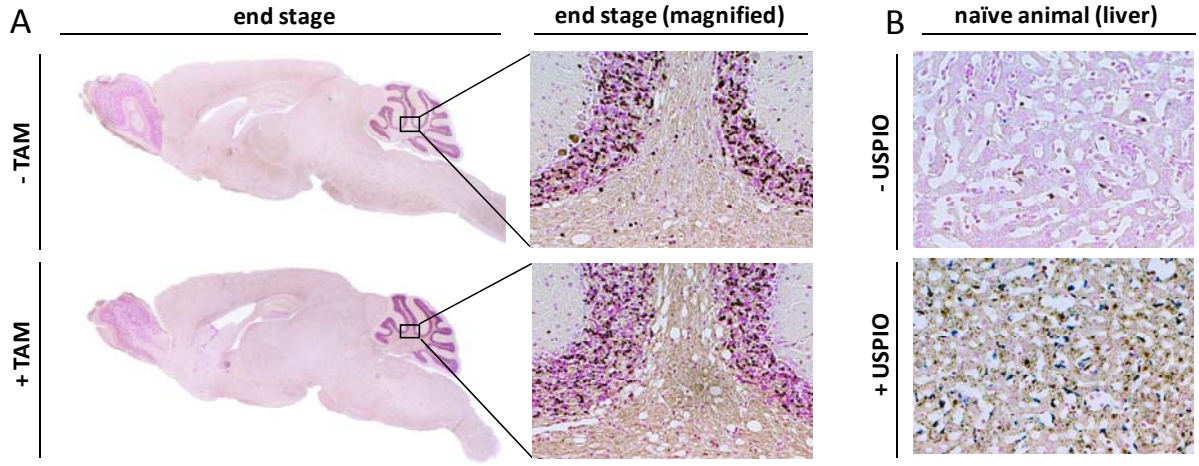

Supplementary Figure 1